2007

GeV-scale electron acceleration in a gas-filled capillary discharge waveguide

Stefan Karsh
Max-Planck-Institut für Quantenoptik, stefan.karsch@mpq.mpg.de

J. Osterhoff
Max-Planck-Institut für Quantenoptik

A. Popp
Max-Planck-Institut für Quantenoptik

T.P. Rowlands-Ree
University of Oxford

Zs. Major
Max-Planck-Institut für Quantenoptik

See next page for additional authors

New Journal of Physics
The open–access journal for physics

GeV-scale electron acceleration in a gas-filled capillary discharge waveguide

S Karsch[1,6], J Osterhoff[1], A Popp[1], T P Rowlands-Rees[2], Zs Major[1], M Fuchs[1,3], B Marx[1,3], R Hörlein[1,3], K Schmid[1,3], L Veisz[1], S Becker[3], U Schramm[4], B Hidding[5], G Pretzler[5], D Habs[3], F Grüner[1], F Krausz[1,3] and S M Hooker[2]

[1] Max-Planck-Institut für Quantenoptik, Hans-Kopfermann-Str. 1, D-85748 Garching, Germany
[2] Clarendon Laboratory, University of Oxford, Parks Road, Oxford OX1 3PU, UK
[3] Sektion Physik der Ludwig-Maximilians-Universität München, Am Coulombwall 1, D-85748 Garching, Germany
[4] Forschungszentrum Dresden-Rossendorf, Bautzner Landstr. 128, D-01328 Dresden, Germany
[5] Institut für Laser- und Plasmaphysik, Heinrich-Heine-Universität, Universitätsstr. 1, D-40225 Düsseldorf, Germany
E-mail: stefan.karsch@mpq.mpg.de

New Journal of Physics **9** (2007) 415
Received 14 September 2007
Published 23 November 2007
Online at http://www.njp.org/
doi:10.1088/1367-2630/9/11/415

Abstract. We report experimental results on laser-driven electron acceleration with low divergence. The electron beam was generated by focussing 750 mJ, 42 fs laser pulses into a gas-filled capillary discharge waveguide at electron densities in the range between 10^{18} and 10^{19}cm^{-3}. Quasi-monoenergetic electron bunches with energies as high as 500 MeV have been detected, with features reaching up to 1 GeV, albeit with large shot-to-shot fluctuations. A more stable regime with higher bunch charge (20–45 pC) and less energy (200–300 MeV) could also be observed. The beam divergence and the pointing stability are around or below 1 mrad and 8 mrad, respectively. These findings are consistent with self-injection of electrons into a breaking plasma wave.

[6] Author to whom any correspondence should be addressed.

PII: S1367-2630(07)60033-0

Contents

1. Introduction

With the first experimental demonstration of quasi-monoenergetic electron bunches in a laser-plasma acceleration experiment [1]–[3] the vision of Tajima and Dawson [4] of building an ultrahigh-gradient laser-wakefield accelerator has finally become mature enough to be turned into a real world application. Such a laser-driven accelerator might not only be the solution for the size and cost problems of tomorrow's high-energy physics accelerators, but in the more near term might serve as an ideal driver for a table-top x-ray free electron laser (TT-XFEL) [5].

The success in the above experiments came with the realization of the so-called blowout or 'bubble' regime [6], where the laser pulse is intense and short enough to drive the first wake into breaking. In contrast to earlier experiments, in this regime only one wakefield trough is loaded with electrons, whose trajectories in phase space all intersect after a certain propagation length and therefore constitute a monoenergetic beam [7]. Reaching this regime demands laser pulses with an intensity above the wave-breaking intensity $I_{\mathrm{wb}} \propto (\omega_{\mathrm{L}}/\omega_{\mathrm{p}})^{4/3} \propto \lambda_{\mathrm{p}}^{4/3}$, where $\lambda_{\mathrm{p}} = 2\pi c/\omega_{\mathrm{p}}$ is the plasma wavelength and $\omega_{\mathrm{p}} = \sqrt{e^2 n_{\mathrm{e}}/(\epsilon_0 \gamma m_{\mathrm{e}})}$ is the plasma frequency, with e, n_{e} and m_{e} the electron charge, density and mass, respectively [8]. Here, $\gamma = \sqrt{1 + a_0^2/2}$ is the cycle-averaged relativistic factor of the plasma electrons, $a_0 = eE/(m_{\mathrm{e}}\omega_{\mathrm{L}}c)$ is the normalized vector potential, E is the laser field, c is the speed of light and ω_{L} is the laser frequency. Furthermore, the transverse and longitudinal laser-beam size should be approximately equal [9] and smaller than half the plasma wavelength. Thus, a long laser pulse should only be focussed to a large spot diameter, in turn limiting its intensity. Working with longer pulses can be compensated for by using a low density with a longer plasma wavelength, but implies a larger focal spot (in length and diameter $\propto \lambda_{\mathrm{p}}^3$) with more intensity ($\propto \lambda_{\mathrm{p}}^{4/3}$), such that the laser energy grows $\propto \lambda_{\mathrm{p}}^{13/3}$. This constrains the pulse duration to less than 30 fs if the laser energy is kept at the joule level. Corresponding plasma densities are in the $10^{18}\,\mathrm{cm}^{-3}$ range. Although self-compression and relativistic self-focussing can compress an initially too long and weak pulse enough to drive a bubble in higher densities [10], the instability of these processes makes short pulses highly desirable. Moreover, in gas-jet experiments the interaction length is often too short for both self-focussing and strong acceleration. In a capillary discharge waveguide both a long interaction length and guiding in a preformed density profile help to overcome these limitations, such that electrons can be effectively accelerated up to the dephasing limit. The dephasing length is defined by the distance L_{deph} over which trapped electrons outrun the plasma wave [11], and

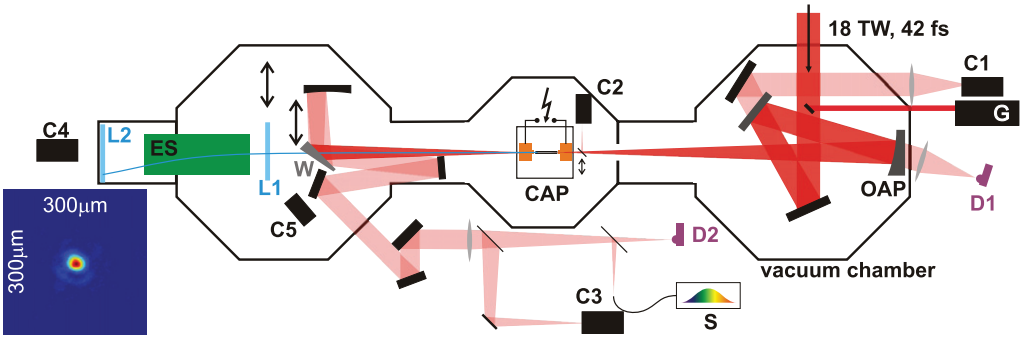

Figure 1. The experimental set-up: G: GRENOUILLE; C1–C5: cameras; D1, D2: diodes; L1, L2: scintillating screens; S: spectrometer; W: wedge; OAP: off-axis-parabola; CAP: capillary waveguide. The inset shows the incoming laser focus at the capillary entrance.

is given in linear approximation by $L_{\mathrm{deph}} = \lambda_{\mathrm{p}}^3/\lambda^2 \propto n_{\mathrm{e}}^{-3/2}$ with the laser wavelength λ. The electrons experience an accelerating electric field of $E_{\mathrm{p}} \propto n_{\mathrm{e}}^{1/2}$ in the plasma wave for $a_0 \sim 1$. Hence, the energy which the electrons can gain by propagating over one dephasing length is $W \approx E_{\mathrm{p}} L_{\mathrm{deph}} \propto n_{\mathrm{e}}^{-1}$. Therefore, a low plasma density as well as a long acceleration length is preferable for accelerating a high-energy electron beam. A gas-filled capillary discharge waveguide [12, 13] can ideally provide these conditions, within the limits discussed above. Recently, the generation of quasi-monoenergetic 1 GeV electrons with 40 TW laser pulses has been demonstrated in such a guiding structure [14, 15].

For the applications mentioned above the reproducibility of the electron beam is of crucial importance. In that context, we report our findings from an experiment similar to that in [14, 15], where electron acceleration was studied in a regime just above the threshold for injection of electrons into the wakefield. As a result, the electron-generation properties were very sensitive to the laser conditions. Owing to the relatively low charge of the electron beams in our case, the space-charge forces and consequently the divergence are very low. We describe the guiding process in the capillary waveguide and also present data on the spatial and spectral properties of the transmitted laser beams. The investigation of the influence of the laser-pulse duration on the electron beams and their correlation with the electron-acceleration process will be discussed in addition. We also present results on the directional stability of the electron beam.

2. Experimental set-up

In our experiment (set-up see figure 1), the upgraded ATLAS Ti:sapphire laser at the Max-Planck-Institut für Quantenoptik delivered 18 TW laser pulses with a duration of 42 fs and an energy of up to 750 mJ at the entrance of the capillary discharge waveguide CAP. In the first chamber, a 1.5 m focal length off-axis parabola (OAP) focussed the laser pulses into a near-diffraction-limited spot with a Strehl ratio of >0.7 and a diameter of 23 μm full width at half maximum (FWHM). This amounted to a vacuum focal intensity of 1.5×10^{18} W cm^{-2} and a normalized field amplitude $a_0 = 0.84$. A removable pick-off mirror took a part of the beam through a thin window into a GRENOUILLE device G for measuring the pulse duration and

phase. The leakages through mirrors were focussed onto an energy- and time-monitoring diode D1 and a pointing camera C1, respectively.

The middle chamber housed the capillary waveguide CAP [12] and a camera C2 equipped with a flip-mirror to check the quality of the laser focus. The capillary had an inner diameter of 200 μm and a length of 15 mm. It was filled with hydrogen through a pulsed valve at backing pressures of up to 600 mbar. A 2.6 nF capacitor charged to 20 kV was discharged through the capillary via a thyratronto create a plasma column waveguide. A Rogowski coil was used to monitor the temporal behaviour of the discharge current.

The evolution of the transverse density profile of the plasma is described elsewhere [16, 17]. During the discharge a temperature gradient is created between the hot core and the cold capillary wall, which leads to a transient concave density profile across the capillary cross-section. This profile acts like a transient positive lens and can confine the incoming laser pulse over a distance longer than its confocal length, which in the present experiment was 2.4 mm. Therefore, in order to guide the laser beam efficiently and access the regime of electron acceleration, careful alignment of the laser through the capillary was necessary, as well as setting the correct timing between the discharge and the laser pulse to ensure the overlap in space and time between the laser and the guiding structure.

The electron beam emerging from the plasma channel could be observed in two different locations along its path. First a CAWO OG16 scintillating screen L1 imaged by a 12-bit camera C5 was used for detecting the beam pointing and divergence at 1.12 m behind the capillary exit. By removing L1 the electrons could enter a 37 cm long permanent dipole magnet spectrometer ES with a nearly homogeneous field of 0.45 T without being scattered. A second CAWO screen L2 read out by a 12-bit camera C4 was used for detection. The fluorescence signal was cross-calibrated with imaging plates [18] to give an absolute charge readout. Three-dimensional particle tracking calculations using the mapped field were applied to calibrate the spectrum and the transverse focussing behaviour.

After the capillary, the transmitted laser beam could be picked-off by a translatable wedge W in order to be relayed onto the diagnostics table. After W the beam was collimated, directed out of the chamber and focussed with an achromatic lens. It was split onto a 12-bit camera C3 to image the capillary exit, a fibre-coupled spectrometer S recording the spectrum, and a PIN diode D2 measuring the transmitted energy.

3. Guiding performance

In our experiments, the guiding performance was strongly linked to the electron acceleration behaviour. For a complete picture, we will therefore give a qualitative interpretation for the characteristics of guiding and laser-energy transport through the capillary in the case of weakly relativistic laser pulses, i.e. $a_0 \sim 1$.

The transmitted energy fraction T, deduced from the ratio of the readings of D1 and D2, versus the delay between the measured onset of the discharge current and the laser-arrival time at the capillary entrance is recorded using full-energy laser shots. The characteristic features in the temporal shape of the guiding curve, i.e. an initial drop, followed by a sudden rise in transmitted laser energy which afterwards decreases slowly, can be observed independently of the pressures used. However, for different pressure settings, the exact timescales of these regions and the obtained transmission values vary. For laser pulses of sufficiently high power, the shape of the guiding curve seems to be dictated by a complex interplay between the lens action of

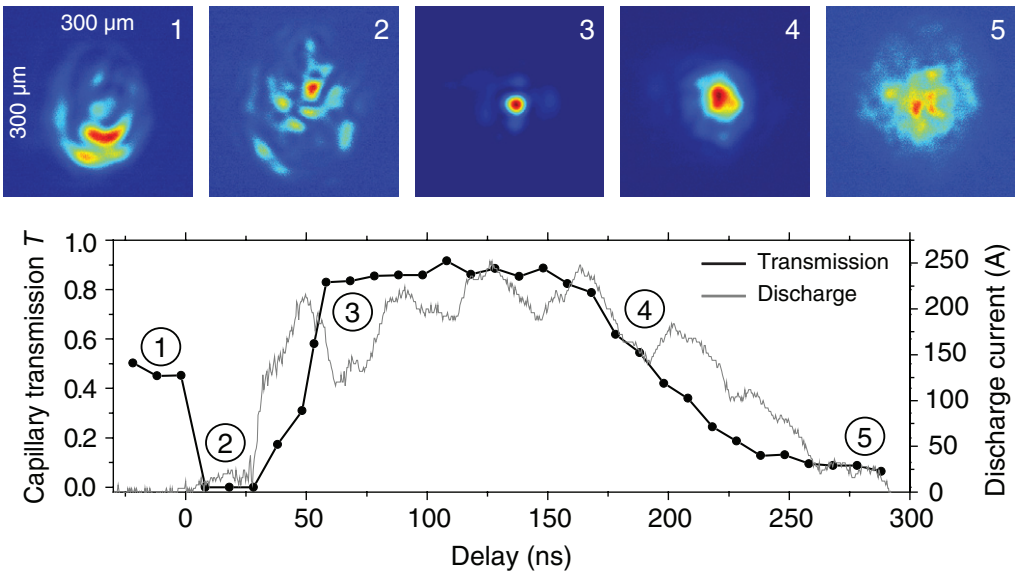

Figure 2. Guiding curve at 100 mbar gas pressure resulting in a mean density of 5×10^{18} cm^{-3} (2.3×10^{18} cm^{-3} on-axis at best guiding) and corresponding discharge current as a function of the delay between its measured onset and the arrival time of the laser pulse at the capillary entrance. The 300×300 μm^2 insets show the guided pulse profiles.

the plasma profile and the relativistic self-focussing of the laser pulse. In figure 2, the guiding curve is shown for low initial pressure (100 mbar $\equiv 5 \times 10^{18}$ cm^{-3} mean density) to illustrate clear guiding behaviour, however, no electron acceleration was observed under these conditions. In order to enhance our understanding of the processes involved, we view this guiding curve in correlation to spectra of the transmitted laser beam (figure 3) taken at slightly higher gas pressure (200 mbar $\equiv 1 \times 10^{19}$ cm^{-3} mean density), where accelerated electron beams were observed.

Under our conditions, the critical power for self-focussing (17 GW $(\omega_L/\omega_p)^2$) is exceeded for plasma densities above 1.9×10^{18} cm^{-3}, which is always the case when in our experiment electron acceleration takes place.

Alongside the guiding curve, figure 2 also shows images of the transmitted laser spot at the capillary exit recorded in the same run.

Long before the discharge (region 1), the laser transmission is ≈50% and the transmitted spot is strongly diffracted. The spectrum in figure 3 displays moderate broadening. This behaviour can be explained by a certain amount of self-focussing and the excitation of a weak wakefield in a laser-ionized plasma with the initial (atomic) gas density. The self-focussing reaches an equilibrium as soon as the relativistic electron mass increase raises the self-focussing threshold above the laser power [19], which prevents the wakefield to be driven into breaking. The laser loses energy and diffracts.

In region 2, the transmitted beam profile becomes significantly distorted and the transmission drops to almost zero owing to initial non-uniformities in the plasma-density profile during the breakdown phase of the discharge.

In region 3, the transmitted laser energy fraction increases strongly and reaches a plateau at 0.95. The pulse is guided with a low-order transverse mode similar to the input mode (cf figure 1). The transmitted laser spectrum for the corresponding region shown in figure 3

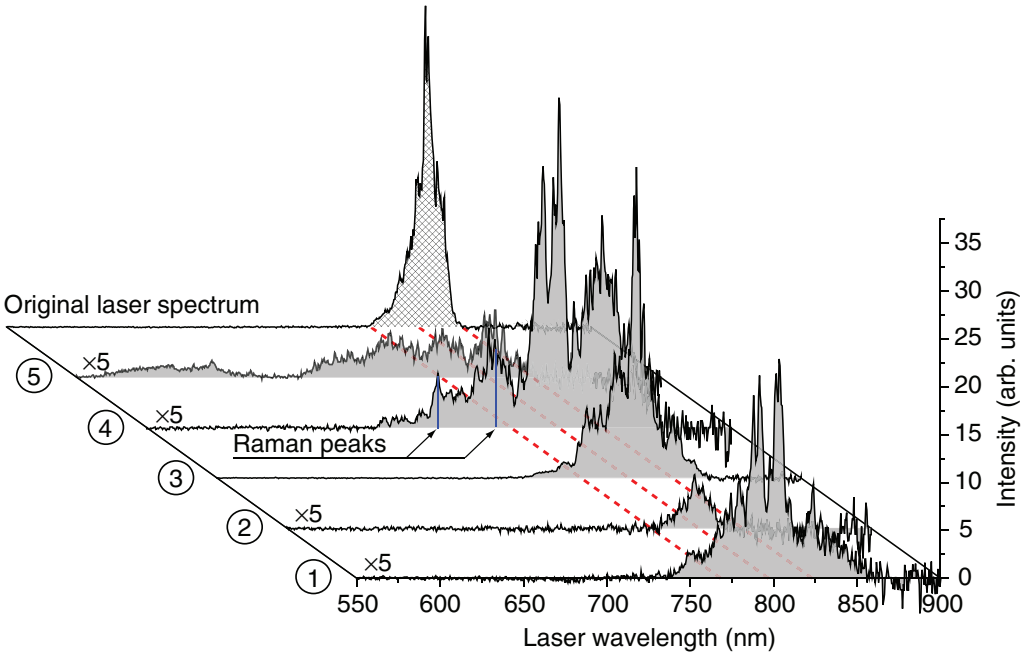

Figure 3. Typical laser spectra for different regions of the guiding curve. The spectrum of the incoming laser pulse is also shown for reference. The dashed (red) lines indicate the centre and full width of this original spectrum. In spectrum 4, the Raman peaks are indicated. Note that the curves for regions 1, 2, 4, 5 are magnified by a factor of 5.

rules out any strong wakefield excitation by its moderate broadening and absence of any obvious Raman satellites. A possible explanation of these findings can be given as follows. During the rise in transmission the initially chaotic distribution evolves into a guiding channel with a parabolic density profile. Simultaneously, the on-axis density drops from the initial value of 5×10^{18} down to 2.3×10^{18} cm^{-3} [16], which is close to the relativistic self-focussing threshold. In contrast to region 1, this lower density leads to a larger self-focussed equilibrium spot size, less energy depletion and less spectral broadening, resulting in efficient guiding even at these high peak laser powers. From the experimental findings and this picture, we may assume that the laser intensity has not reached wave-breaking intensity anywhere along the capillary.

Later in the discharge (region 4), the transmitted laser energy starts to decrease. At higher densities (in our experiment above 140 mbar corresponding to 3.2×10^{18} cm^{-3} on axis), electron acceleration occurs in this region, meaning the pulse intensity must have become sufficiently large to break the plasma wave and inject electrons. Strong indication for the intensity increase is the corresponding spectrum in figure 3, where significant broadening and the onset of Raman satellites at $\pm\omega_p$ are observed. The change in behaviour between regions 3 and 4 is likely to be caused by the evolution of the state of the plasma channel, such as changes in the ionization state or in the transverse or longitudinal profile of the channel. For a better understanding, it is the subject of ongoing PIC-simulations.

At even later times (region 5) during the decrease of the discharge current, a strong ionization blue-shift is observed [20], as can be seen in figure 3. This may indicate that partial recombination of the gas column already occurs before the arrival of the laser pulse.

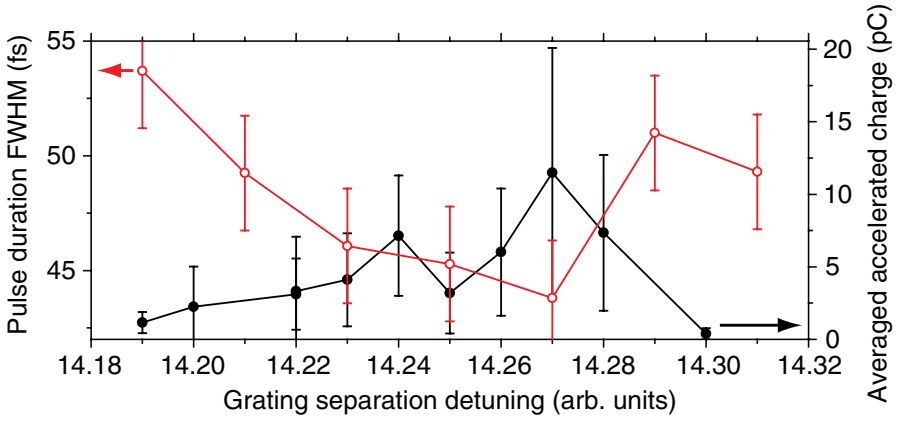

Figure 4. Amount of accelerated charge above 100 MeV and FWHM laser pulse duration as a function of grating separation in the pulse stretcher at an on-axis density of 5×10^{18} cm^{-3}.

As mentioned above, the discussed regions can also be identified for higher pressures. Here, the guided spot quality deteriorates, because the equilibrium spot size becomes smaller and the laser energy is depleted earlier, leading to subsequent defocussing. Also, the collapse into a filament and electron acceleration occurs earlier in the channel evolution due to stronger self-focussing and smaller matched spot size of the plasma channel, leading to a shortening of region 3 and an expansion of region 4.

4. Electron spectra

After discussing the qualitative picture of the guiding behaviour in the capillary in section 3, we will now turn to the investigation of the accelerated electron beams. As mentioned, in region 4 of the guiding curve a wakefield is excited as a consequence of the plasma-density profile and relativistic self-focussing. If the pressure is increased, plasma-wave breaking, injection and trapping of electrons in the wake is induced. In our experiment, the threshold above which electron acceleration occurred was around 140 mbar (corresponding to an on-axis density of 3.2×10^{18} cm^{-3}), and electron beams were observed on the down slope of the laser transmission curve (cf figure 2 region 4). It should be mentioned that the pressure threshold for lower laser powers (slightly longer pulses and/or lower energy) is shifted up, such that with $\approx$20% reduction in laser power no electrons were seen at pressures below 600 mbar. We are therefore operating very close to the threshold of the acceleration regime. This is illustrated in figure 4, where the mean accelerated charge above 100 MeV is plotted against the laser-pulse duration for an on-axis density of 5×10^{18} cm^{-3}. It is clear that the accelerated charge is maximized when the duration of the laser pulse is a minimum, and that even small changes in the pulse duration have a strong effect on the acceleration process.

Figure 5 shows a number of typical images detected on L2 (after removing L1 and W) in the electron-acceleration regime at relatively high densities, i.e. above 1×10^{19} cm^{-3} on the laser-propagation axis. Here, almost every shot produced an electron beam, however, the shot-to-shot fluctuations in energy distribution and accelerated charge were significant. In some cases, accompanying the main electron peak in the few-hundred-MeV range, distinct electron features

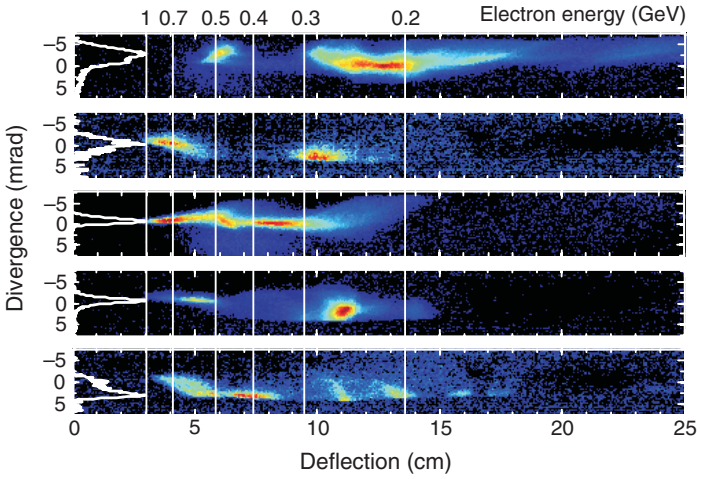

Figure 5. CAWO screen images (L2) for shots at 1×10^{19} cm^{-3} on-axis density, showing features above 500 MeV. On the left, the lineout through the highest energy prominent features are plotted, showing their divergence.

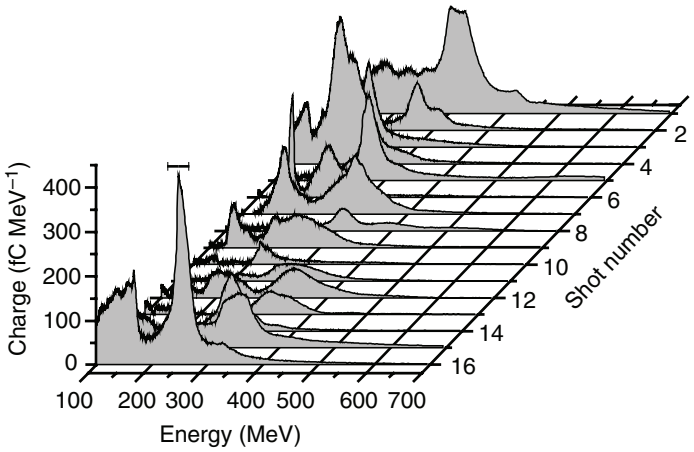

Figure 6. Electron spectra extracted from the scintillating screen images for shots at 5×10^{18} cm^{-3} on-axis density. The charge/MeV is given on the vertical axis. Due to the finite size of the spectrometer opening, the pointing fluctuations introduce an energy uncertainty, which amounts to $\pm$21 MeV at 260 MeV (shot #16) and is a strictly increasing function of the energy.

were detected at positions corresponding to 0.6–1.0 GeV. Owing to the poor spectrometer resolution, in an extracted spectrum these features would be smeared out over a large range of energies, containing the contributions from divergence, energy spread and instrument-transfer function. In order to give a first-hand impression of these features, the direct images are shown in figure 5 along with the energy calibration. Although most of the electrons are accelerated to lower energies around 300 MeV, features above 500 MeV contain several picocoulomb of charge.

When lowering the on-axis electron density in the capillary to values around 5×10^{18}cm^{-3}, the characteristics of the accelerated electron bunches change in the following ways. In figure 6,

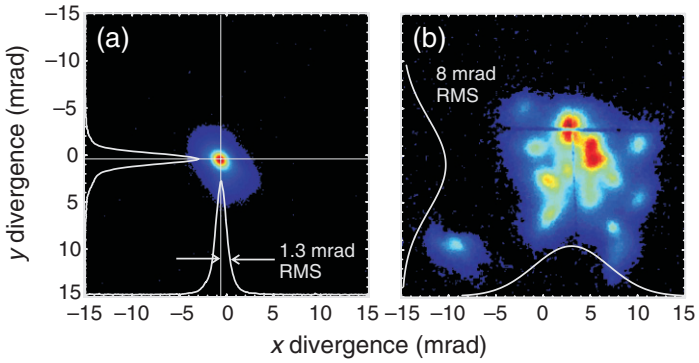

Figure 7. (a) Image of a typical electron bunch on screen L1. The lineouts through the peak indicate a divergence of 1.3 mrad in this particular case. (b) Sum of 27 individual shots as shown in (a) as an indication of shot-to-shot pointing errors. The gaussian curves are a fit to the distribution of the beam centroids. The dark cross is caused by markings on the CAWO screen. Both (a) and (b) were taken at 6.7×10^{18} cm^{-3} on-axis density.

spectra from one run at this pressure are plotted, showing accelerated electron bunches with a much higher energy stability compared to the high-density regime. Strongly peaked spectra with $<$20% energy spread are detected on almost every shot in the range from 200 to 300 MeV. In addition to the improved stability, the typical values for the total accelerated charge range from 20 to 45 pC (e.g. in the case of shot #1). Finding a regime in our parameter space allowing for stable electron acceleration with as much bunch charge as possible is crucial if applications such as TT-XFEL [5] are considered. Therefore, the trend towards higher stability when the gas density is lowered is an encouraging result of our experimental set-up. However, by lowering the density even further, we eventually reach the threshold below which no electron acceleration can take place due to the absence of electron injection into the accelerating wakefield structure. In other works, this limitation is overcome by either controlled electron injection [21], or careful control of laser parameters combined with higher powers [15]. In the future, a power upgrade of the ATLAS system will enable us to follow the latter route.

5. Electron beam divergence and pointing

In addition to the energy characteristics of the electron bunches, we investigated their divergence and pointing stability, which are also of great importance for future applications. Under ideal conditions, $>$90% of all laser shots generated an electron beam, which could be observed on screen L1 with the wedge W removed. At the position of the screen, the RMS divergence of a typical shot is $\sim$1–2 mrad (see figure 7(a)). As clarified in figure 8, the larger divergence halo is formed by the low-energy tail of the electron bunch, whereas the high-energy part mainly contributes to the central peak. Here, the images of the scintillating screen L2 are displayed for three selected shots at 8.4×10^{18} cm^{-3} on-axis density. An ultra-compact, monoenergetic bunch of down to sub-mrad divergence is surrounded by a broad-band, higher-divergence halo.

Figure 7(b) shows the sum of 27 individual electron-beam images of the scintillating screen L1, giving an indication of the shot-to-shot pointing fluctuations. A gaussian fit to the distribution of the individual beam centroids (also shown in figure 7) gave an RMS pointing

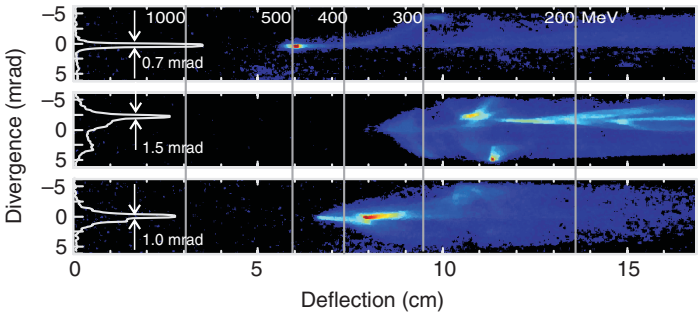

Figure 8. Transverse beam profile versus magnetic deflection in the spectrometer plane for shots at 8.4×10^{18} cm^{-3}. The lineouts are taken through the highest-energy peak and give an impression of the transverse size of the quasi-monoenergetic bunches.

error of ∼8 mrad. Each single electron bunch signal on L1 was compared with the corresponding pointing of the laser pulse into the capillary for the same shot, but no correlation was found. The pointing variations may arise from fluctuations in the near-field profile of the laser, which effectively causes pointing deviations from the optical axis or shot-to-shot instabilities inside the plasma channel.

From the analysis of a large number of shots, a trend to larger divergence with higher charge can be noticed, however, this remains the subject of further studies. Also, higher pressure runs tend to produce smaller electron beams with less charge and sometimes more than one peak, while at lower pressure the divergence and charge are higher. This behaviour can be explained by the stronger focussing forces and smaller bubble volume for higher pressure, along with a possible break-up of the laser beam in filaments and/or multiple peaks. In agreement with [14, 15] and in contrast to other experiments [1]–[3] we also observed such multiple peaks in our electron spectra (cf figures 5 and 6). The plasma period for the densities used for electron acceleration in our experiment ranges from ∼40 to ∼70 fs, which is close to the laser-pulse duration. Under these conditions, the laser can break up and drive a succession of two or more bubbles. Our available laser power dictates the use of such high densities in order to achieve wave breaking, which are not fully matched to the laser-pulse duration.

6. Conclusion

We accelerated electrons to GeV-scale energies in a capillary discharge waveguide using 18 TW, 42 fs laser pulses. Our observations are in agreement with the experiments of Leemans *et al* [14], which were performed in a similar regime with more energetic laser pulses and generated quasi-monoenergetic electron bunches at 0.5 and 1 GeV with 25 and 40 TW laser powers, respectively. We present data on shot-to-shot reproducibility of the accelerated electron beams and suggest a possible scenario for the guiding behaviour in the case of weakly relativistic laser pulses. Although the measured divergence to our knowledge is the smallest reported so far for a laser-driven acceleration experiment, the divergence and the pointing variations we have identified are still an order of magnitude above the requirements for e.g. a TT-XFEL. We believe that these fluctuations are largely caused by the fact that we are operating so close to the threshold of self-focussing and electron injection, such that a moderate increase in laser power will significantly improve the stability.

Acknowledgments

We thank J Meyer-ter-Vehn and M Geissler for fruitful discussions. The work was funded by the Max-Planck Society and the DFG through GRK1203, the Transregio 18 and the MAP Cluster of Excellence funding schemes. Financial support from the Marie-Curie Individual Fellowship No. MEIF-CT-2005-024150 (ZsM) is also acknowledged. TRR appreciates the support of a studentship funded by the Engineering and Physical Sciences Research Council, UK.

References

[1] Faure J, Glinec Y, Pukhov A, Kiselev S, Gordienko S, Lefebvre E, Rousseau J-P, Bourgy F and Malka V 2004 *Nature* **431** 541
[2] Mangles S P D *et al* 2004 *Nature* **431** 535
[3] Geddes C G R, Tóth Cs, van Tilborg J, Esarey E, Schroeder C B, Bruhwiler D, Nieter C, Cary J and Leemans W P 2004 *Nature* **431** 538
[4] Tajima T and Dawson J M 1979 *Phys. Rev. Lett.* **43** 267
[5] Gruener F *et al* 2007 *Appl. Phys.* B **86** 431
[6] Pukhov A and Meyer-ter-Vehn J 2002 *Appl. Phys.* B **74** 355
[7] Geissler M, Schreiber J and Meyer-ter-Vehn J 2006 *New J. Phys.* **8** 186
[8] Bulanov S V, Yamagiwa M, Esirkepov T Zh, Koga J K, Kando M, Ueshima Y, Saito K and Wakabayashi D 2006 *Phys. Plasmas* **12** 073103
[9] Gordienko S and Pukhov A 2005 *Phys. Plasmas* **12** 043109
[10] Hidding B *et al* 2006 *Phys. Rev. Lett.* **96** 105004
[11] Sprangle P, Esarey E, Ting A and Joyce G 1988 *Appl. Phys. Lett.* **53** 2146
[12] Spence D J and Hooker S M 2001 *Phys. Rev.* E **63** 015401
[13] Butler A, Spence D J and Hooker S M 2002 *Phys. Rev. Lett.* **89** 185003
[14] Leemans W P, Nagler B, Gonsalves A J, Tóth Cs, Nakamura K, Geddes C G R, Esarey E, Schroeder C B and Hooker S M 2006 *Nat. Phys.* **2** 696
[15] Nakamura K, Nagler B, Tóth Cs, Geddes C G R, Schroeder C B, Esarey E, Leemans W P, Gonsalves A J and Hooker S M 2007 *Phys. Plasmas* **14** 056708
[16] Gonsalves A J, Rowlands-Rees T P, Broks B H P, van der Mullen J J A M and Hooker S M 2007 *Phys. Rev. Lett.* **98** 025002
[17] Rowlands-Rees T P and Hooker S M, to be published
[18] Tanaka K A, Yabuuchi T, Sato T, Kodama R, Kitagawa Y, Takahashi T, Ikeda T, Honda Y and Okuda S 2005 *Rev. Sci. Instrum.* **76** 013507
[19] Brandi H S, Manus C, Mainfray G and Lehner T 1993 *Phys. Rev.* E **47** 3780
[20] Rae S C and Burnett K 1992 *Phys. Rev.* A **46** 1084
[21] Faure J, Rechatin C, Norlin A, Lifschitz A, Glinec Y and Malka V 2006 *Nature* **444** 737